Available online at www.sciencedirect.com

ScienceDirect

journal homepage: www.elsevier.com/locate/he

# $H_2$ from biofuels and carriers: A concerted homo-heterogeneous kinetic model of ethanol partial oxidation and steam reforming on $Rh/Al_2O_3$

*Vittoria Troisi* [a,1], *Veronica Piazza* [a,1], *Alessandro Stagni* [b], *Alessio Frassoldati* [b], *Gianpiero Groppi* [a], *Alessandra Beretta* [a,*]

[a] *Laboratory of Catalysis and Catalytic Processes, Dipartimento di Energia, Politecnico di Milano, via La Masa 34, 20156 Milano, Italy*

[b] *CRECK Modeling Group, Dipartimento di Chimica, Materiali e Ingegneria Chimica, Politecnico di Milano, Piazza Leonardo da Vinci 32, 20133 Milano, Italy*

## HIGHLIGHTS

- A 36-species reduced homogeneous model is validated against gas-phase tests.
- A heterogeneous kinetic scheme for ethanol CPO and SR on $Rh/Al_2O_3$ is developed.
- C-poisoning explains hindered kinetics of ethanol SR, in line with Raman and TPO.
- The combined homo-heterogeneous model describes a wide experimental field.

## GRAPHICAL ABSTRACT

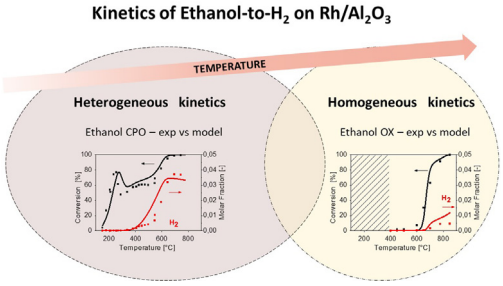


## ARTICLE INFO

*Article history:*
Received 18 July 2022
Received in revised form
7 February 2023
Accepted 12 March 2023
Available online 13 April 2023

*Keywords:*
Hydrogen
Ethanol

## ABSTRACT

Investigating bioethanol as a renewable energy source is crucial in the context of $H_2$-based economy. Ethanol partial oxidation and steam reforming on $Rh/Al_2O_3$ represent promising processes that have already proved to be highly tangled reacting systems.

In this work, a significant step forward has been done towards the development of an engineering tool that can capture all the relevant features of the process; a combined homo-heterogeneous kinetic scheme was developed and validated against experimental data, informative of the catalytic and thermal activation of the $C_2$-alcohol.

In particular, a 36-species reduced homogeneous scheme was developed, able to capture observed trends with a limited computational load. On the other side, a macro-kinetic heterogeneous scheme with six molecular reactions (ethanol oxidative dehydrogenation,

* *Corresponding author.*
E-mail address: alessandra.beretta@polimi.it (A. Beretta).

[1] Vittoria Troisi and Veronica Piazza equally contributed to the manuscript.

https://doi.org/10.1016/j.ijhydene.2023.03.178

$Rh/Al_2O_3$
Homogeneous kinetic model
Heterogeneous kinetic model
Annular reactor

total oxidation, decomposition, dehydrogenation, steam reforming and acetaldehyde post-reforming) was tuned to accurately describe ethanol/$O_2$ and ethanol/$H_2O$ reacting systems.


## Introduction

The study of Catalytic Partial Oxidation (CPO), Steam Reforming (SR) and catalytic cracking of sustainable energy vectors is of particular interest in the perspective of a future $H_2$-driven economy. Efforts are focused on the development of efficient catalytic processes, able to convert liquid fuels and $H_2$-vectors into $H_2$-rich streams. In this context, synthetic green carriers (e.g. e-$NH_3$) and biomass-derived fuels represent the most promising candidates for the distributed production of zero- or low-C hydrogen.

The consolidated role of bioethanol in the transportation sector makes it an interesting choice for stationary and on-board applications, because of its abundant availability from inedible biomass such as energy crops, agricultural or forest waste and residues. In this view, some of the authors have recently studied ethanol CPO and SR on $Rh/Al_2O_3$ catalyst [1]: the combination of catalytic testing, Raman spectroscopy, *operando* FTIR and TPO analyses allowed to reveal the full complexity of this reacting system, composed of multiple reaction pathways; herein $H_2$ production routes are hindered by the strong adsorption of surface C-species at temperatures below 500 °C, but above this threshold surface reactions gain a high temperature sensitivity and $H_2$ production becomes highly selective.

Previous studies have addressed the development of heterogeneous kinetic schemes of ethanol partial oxidation or steam reforming on noble metal-based catalysts like $Rh/Al_2O_3$, that are preferred candidates for process intensification and on-board applications due to their higher activity when compared to transition metals; additionally, noble metals have shown a higher resistance to C-deposition, a key property when oxygenates are involved [2]. Vaidya et al. studied ethanol reforming on a commercial $Ru/Al_2O_3$ in a traditional fixed bed reactor over a narrow temperature range (600–700 °C), estimating an apparent activation energy of 96 kJ/mol [3]. Görke and co-authors carried out their investigation on ethanol reforming in a microreactor and were able to extend the temperature window of analysis (350–660 °C) [4]; they used $Rh/CeO_2$, a catalyst characterized by a low acidity that inhibited the onset of coking. Graschinsky et al. showed that the rate-determining step (RDS) of ethanol steam reforming on Rh(1%) $MgAl_2O_4/Al_2O_3$ involves two sites of the same type [5]. Furthermore, it was seen that in the presence of $O_2$ co-feed, oxidation reactions prevail in the inlet part of the reactor and at low temperatures [6]; as a general consequence, the increase in oxygen-to-ethanol ratio in the feed lowers the selectivity to $H_2$ and CO in favour of $CO_2$ [7]. An equivalent behaviour was observed in Ref. [8], where a detailed reaction mechanism for ethanol CPO on Pt–Rh supported catalysts is proposed.

Surprisingly, in-depth studies on the effect of C-poisoning on ethanol reaction kinetics remain extremely scarce.

Moreover, literature studies do not account for the possible ignition of homogeneous reactions, that can occur in the high temperature range and can compete with catalytic pathways.

Several detailed homogenous kinetic mechanisms are available in literature. Nowadays, it is recognized that the information contained in detailed chemistry is necessary to guarantee the accuracy of large-scale simulations [9]. Yet, it is often not applicable "as such" in multidimensional simulation tools due to the number of species to be transported. Most of the CPU time in the integration of the ordinary differential equations (ODEs) describing a reacting systems is spent in the factorization of the associated Jacobian matrix [10]: the time complexity of this step scales with $n^p$, with $n$ being the number of equations, and $p = 3$ for several adopted algorithms [11]. For this reason, mechanism reduction is a suitable approach to facilitate practical simulations using realistic chemistry with modern computational tools, as it reduces the number of species to be transported, thus the resulting size of the Jacobian.

Starting from this background, the main objective of the present manuscript is to develop both a reduced homogeneous and a lumped heterogeneous kinetic scheme of the ethanol conversion routes on Rh, thus setting the engineering tools necessary for the design of catalytic reactors and the development of ethanol-to-$H_2$ technologies. In view of a dedicated modelling analysis for the optimization of $H_2$ production from ethanol in an autothermal reformer (presently ongoing), the necessity to combine the description of both solid and gas phase reactivities appears essential, being the latter of utmost importance in the typical operating temperatures of the fuel processor [12]. At this scope, an experimental campaign in annular microreactor was focused on the obtainment of kinetically relevant data in a wide operating field.

## Experimental methods

### *Catalyst preparation*

Catalytic experiments were performed on 2 wt% $Rh/\alpha$-$Al_2O_3$ catalysts, which were prepared following a procedure developed in previous works [13–15]. $\alpha$-$Al_2O_3$ powders were obtained by calcining commercial $\gamma$-$Al_2O_3$ (SASOL PURALOX SCFa 140 or SBa 200) in air at 1100 °C for 10 h; in this way, a support stable at the operating temperatures typical of an autothermal fuel processor (above 800 °C) was obtained. Rhodium was added via incipient wetness impregnation, using an aqueous solution of $Rh(NO_3)_3$ and then catalytic

powders were dried in oven at 120 °C for 3 h. Superficial area of 8 $m^2$/g and pore volume of 0.21 $cm^3$/g were measured via BET (TriStar Micrometrics 3000) and Hg-porosimetry (MicroActive AutoPore V), while ICP-MS (X Series II by Thermo Fisher) and $H_2$-chemisorption (ThermoQuest TPD/R/O1100) analyses revealed a real Rh load on the support of 2.3 wt% and 30% dispersion, respectively. Previous XRD and FESEM studies exhibit the presence of Rh nanoparticles dispersed on $Al_2O_3$ with a diameter in the range of 2–25 nm [1]; further analyses on spent catalytic samples also confirm that these Rh particles are not subjected to sintering in the explored operating conditions, as shown in Supplementary Material S1.

A slurry was then prepared by dispersing catalytic Rh/$\alpha$-$Al_2O_3$ powders in an acidic solution ($HNO_3$/powder = 1.7 mmol/g, $H_2O$/powder = 1.4 mL/g) and by a 24 h-milling treatment, where zirconia balls were used [16]. For testing in annular reactor, this slurry was deposited through a dip-coating procedure around dense-alumina tubular supports (O.D. 3.96 mm, 35.5 cm length), in the form of micrometric-thin layers. These alumina tubes present an inner cavity (I.D. 1.98 mm) for the insertion of a thermocouple. Washcoated tubes were subjected to a flash drying in air at 280 °C for 10 min.

Catalytic layers with different lengths (2–6 cm) and washcoat mass (15–60 mg) were prepared and tested for the present work. Before catalyst deposition, a boehmite primer was deposited on the tubular supports to enhance the adherence of the support.

### *Catalytic and gas-phase kinetic tests*

Catalytic experiments were carried out using an annular microreactor, obtained by inserting the catalyst-coated alumina tubes into a quartz reactor with I.D. 5 mm. Homogeneous experiments were also performed by using bare tubes. A tubular Carbolite oven was used to heat the quartz reactor at the desired temperature. Details about this annular microreactor configuration are given elsewhere [16–19].

Gases (Air, $N_2$, $H_2$) were fed with mass flow controllers (Brooks), while a saturator with bubbling $N_2$ was used to feed ethanol. For experiments with $H_2O$ co-feed, water was instead synthesized in an upstream Pt/$Al_2O_3$ reactor, by sending a diluted mixture of $H_2$ (in 5% v/v excess) and stoichiometric $O_2$. Composition measurements of inlet and outlet mixtures were carried out in an online micro-GC (Agilent Technologies, 3000 A), provided with two capillary columns (Molecular Sieve for $H_2$–$O_2$–$N_2$–$CH_4$–CO, PoraPlotU for $CO_2$-ethylene–$H_2O$–acetaldehyde-ethanol) and TCD detectors.

The annular microreactor configuration has already proven its suitability for the fundamental kinetic study of $H_2$ production processes from several hydrocarbons (methane [16,20], propane [21], propylene [22], octanes [23]) and oxygenated fuels (formic acid [24], acetic acid [25]). Indeed, the possibility to use high Gas Hourly Space Velocities (GHSV = $10^5$-$10^6$ NL/$kg_{cat}$/h) without pressure-loss allows to explore a wide temperature window and to study intrinsically fast processes, from low to very high temperatures.

Each Rh/$Al_2O_3$ coated tube was subjected to a conditioning procedure before ethanol experiments, aiming to lead the catalyst to a stable behaviour. The conditioning procedure, consisting of repeated tests of $CH_4$ CPO, has been described in a previous study [14].

All the ethanol experiments were run at atmospheric pressure between 150 and 800 °C, following a stepwise temperature increase (maximum 50 °C). At each temperature, three composition measurements were collected and averaged: moreover, temperature axial profiles were measured by sliding a K-thermocouple inside the inner cavity of alumina tubes, and the average temperature of the catalytic bed was estimated. To illustrate the results in the present work, composition measurements in terms of reactants conversion and products molar fractions are plotted against the average catalyst temperature.

Ethanol CPO experiments were run with inlet ethanol concentration of 0.3–1.5% and $O_2$ concentration of 0.3–1.68%, while using $N_2$ to balance and varying GHSV between $5{\cdot}10^5$ and $2{\cdot}10^6$ NL/$kg_{cat}$/h. Ethanol SR tests were carried out at $0.9–1.5{\cdot}10^6$ NL/$kg_{cat}$/h, feeding 1.5% ethanol and 1–3% $H_2O$. Similarly, homogeneous ethanol oxidation tests were run with 1%–1.5% ethanol and 0 or 1.68% $O_2$, respectively; the total inlet flowrate was varied in an interval (225–1354 NmL/min) corresponding to the range of flowrate investigated in catalytic experiments.

## Mathematical methods

### *Thermodynamic calculations*

Thermodynamic equilibrium calculations were performed at constant temperature and pressure through the STANJAN equilibrium code for the species $C_2H_5OH$, $CH_3CHO$, $C_2H_4$, $CH_4$, $O_2$, $N_2$, CO, $CO_2$, $H_2$, and $H_2O$ [26]. Chemical equilibrium trends were plotted in dot-dashed lines together with experimental data in the following sections.

### *Reactor models*

A quantitative analysis of the catalytic experimental results was realized by means of a steady state 1D, heterogeneous model of the annular reactor, whose governing equations, boundary conditions and transport correlations are reported in dimensionless form in Table 1. The model was broadly discussed and applied in previous works [16,24]. Plug flow mass balances are used for simulating the axial evolution of reacting species in gas phase, while equations of continuity at gas-solid interphase describe solid phase reactivity. Both inter-phase and intra-phase mass transfer phenomena are accounted for: a local Sherwood number is introduced to consider inter-phase mass transfer resistances, while generalized internal effectiveness factor for $O_2$ evaluates the impact of intra-phase mass resistances. Molecular diffusivity was approximated as binary diffusivity of each species in $N_2$, according to the Fuller-Shettler-Giddings correlation [16].

The annular reactor model was successfully used in the past for the kinetic study of $H_2$ production processes on Rh/$Al_2O_3$ and molecular schemes were developed for several fuels ($CH_4$ [16,27], propane [21], propylene [22], octanes [23], formic acid [24]). In the present work, the pre-existing $C_1$-model

**Table 1 – Model equations of annular reactor.**

Mass balance equation of species $i$

$$Pe_{m,i}\frac{dF_i^*}{dz^*} = -\frac{4}{1+\frac{1}{R^*}}Sh_{loc,i}(x_i^B - x_i^W)\frac{F_{TOT}}{F_{TOT}^0} \quad \text{with} \quad R^* = \frac{R_{int}}{R_{ext}}$$

Continuity equation for species $i$

$$Sh_{loc,i}(x_i^B - x_i^W) = \sum_{j=1}^{NR}\nu_{i,j}\alpha_i r_j \quad \text{with} \quad \alpha_i = \frac{d_h \cdot m_{cat}}{S \cdot D_i \cdot C_{TOT}}$$

Mass transfer coefficient

$$Sh_{loc,i} = Sh_{inf} + 6.874e^{-71.2\left(\frac{z^*}{Pe_{m,i}}\right)}\left(1000\left(\frac{z^*}{Pe_{m,i}}\right)\right)^{-0.35}$$

with $Sh_{inf} = 3.11$ [24]

[16,21] was extended to describe ethanol catalytic partial oxidation and steam reforming reactivity on Rh. Inheriting the analysis of the involved chemical pathways carried out by some of the authors in Ref. [1], kinetic dependencies were studied in order to derive the rate laws able to fit a wide set of experimental data.

Gas-phase reactivity was studied by performing simulations using the constant pressure isothermal plug flow reactor code of the OpenSMOKE++ framework [10]. A reactor length of 10 cm (equivalent to an empty reactor volume of 0.7 $cm^3$) was assumed in calculations, corresponding to the isothermal portion of the reactor where temperature profiles were measured.

## Development of a reduced homogeneous kinetic model

The background on homogeneous chemistry of ethanol pyrolysis and oxidation is reported by Ranzi et al. [28]. This mechanism has been updated and is included in a comprehensive $C_1$–$C_3$ high temperature kinetic mechanism (named "CRECK_2003_C1_C3_HT"), that was developed following a hierarchical methodology: the core $C_0$–$C_2$ subset, including ethanol, was taken from the ARAMCO mechanism of Metcalfe et al. [29], while $C_3$ chemistry was taken from Burke et al. [30]. Thermodynamic properties were accounted for from the database of Burcat and Ruscic [31]. The final mechanism includes 114 species and 1999 reactions, and it is available with thermodynamic and transport properties [32].

In this work, the detailed mechanism has been reduced in order to be flexibly applied to simulation of catalytic processes operating under fuel rich oxidation conditions. To this purpose, the methodology described in Ref. [33] was employed, as incorporated in the DoctorSMOKE++ tool. The Directed Relation Graph with Error Propagation (DRGEP) [34] was thus coupled to sensitivity analysis on species [35]. A maximum 10% error on ignition delay time was set as target of accuracy, and 1D homogeneous reactors were used to sample reaction states. The obtained skeletal mechanism included 51 species and 613 reactions. This reduced mechanism was validated against a wide range of existing experimental datasets (jet-stirred reactors, flow reactors, ignition delay times and laminar flame speeds) in order to test the accuracy of the reduction method. Examples of the comparisons between experimental data and model predictions with both the complete and reduced mechanisms are reported in Supplementary Material S2.

As an example, Fig. 1 shows the effect of model reduction in the simulation of the data by Alzueta et al. [36], who studied the oxidation of ethanol in presence of $H_2O$ in an atmospheric laminar flow reactor in the temperature range 700–1500 K ($\lambda = 1.13$) [36].

The reduced model (solid lines) fully replicates the response of the detailed model (dotted lines); both models predict the conversion of ethanol satisfactorily, while underestimate the initial formation of CO and $CO_2$ and show a delay of about 50 K. This reactor was simulated using a plug flow model, i.e. neglecting the possible effect of diffusion on the reactivity of the system. Adopting a plug flow model to simulate a laminar reactor might lead to an underestimation of the reactivity of the order of 25–75 K, as highlighted by Stagni et al. [37] who compared a 2D CFD modelling with a plug flow assumption for the oxidation of DME in a laminar flow reactor. Such a complex modelling activity is outside the scope of this work.

The reduced mechanism could be further reduced to 36 species and 400 reactions (available as supplementary material in. zip package), focusing on the low pressure and high dilution conditions of interest for the simulation of the present catalytic and homogeneous tests.

## Validation of the reduced homogeneous kinetic scheme

The gas phase reactivity of ethanol/$O_2$/$N_2$ mixtures was studied by performing tests at 1.5% ethanol, 1.68% $O_2$ and $N_2$ to balance, by varying inlet flowrate between 225 and 1334 Nml/min in the temperature range 400–850 °C. This set of data represents an additional validation of the homogeneous reduced mechanism, already reported in the Supplementary material S2.

Fig. 2 shows the experimental results (symbols) as well as the predictions of the reduced (solid lines) versus complete (dashed lines) homogeneous mechanism.

In the absence of the catalyst, ethanol conversion starts at 600 °C or even higher temperatures for shorter residence times, thus excluding the influence of homogenous reactions in the low temperature region in the conditions mostly investigated experimentally.

The model predictions describe in a satisfactory way the general trends and provide a key for the interpretation of results. According to the gas-phase mechanism (reaction path analysis in Supplementary Material S3), ethanol is initially consumed via H-abstraction reactions forming mostly the secondary radical ($CH_3CHOH$) which leads to the production of acetaldehyde. The formation of the primary ethanol radical is significant but less important, and leads to the formation of ethylene. Finally, the alcoxy radical is formed in lower amounts and supports the formation of $CH_2O$. The role of molecular dehydration of ethanol to form ethylene is quite small in these conditions. The main homogeneous consumption route of ethanol is thus the following: $C_2H_5OH \rightarrow CH_3CHOH \rightarrow CH_3CHO \rightarrow \ldots \rightarrow CO \rightarrow CO_2$. Acetaldehyde is the primary intermediate species, which at higher

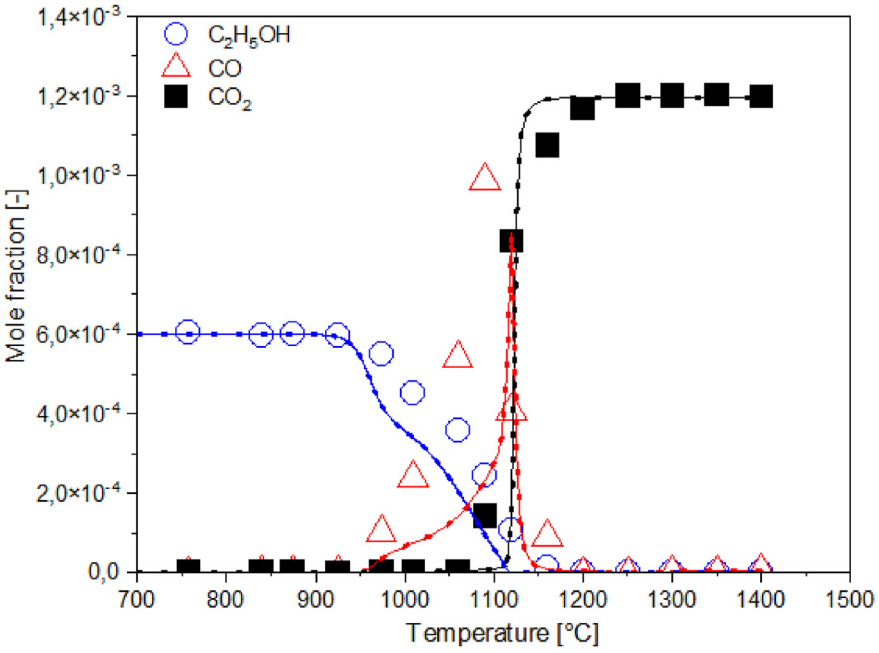


**Fig. 1 – Oxidation of ethanol in atmospheric flow reactor at λ = 1.13 [36]. Comparison between experimental data (symbols), complete model predictions (dotted lines) and 51 species reduced model predictions (solid lines).**

temperatures is consumed to form CO and $CH_3$ (via acetyl radical $CH_3CO$). CO is subsequently oxidized to $CO_2$ by OH radicals. Molecular hydrogen is formed by H-abstraction reactions of H radicals.

Experimental results show that $H_2$ and CO were mainly formed at 700–750 °C, while minor amounts of $CO_2$, and $C_2$ species (ethane and ethylene) were also detected. At decreasing flow rate, the conversion was progressively anticipated and the production of all terminal species grew. The observed trends of acetaldehyde confirmed the character of intermediate species.

Notably, the model predictions tend to partly overestimate syngas production while the concentration of $CO_2$ is underestimated. This has been interpreted as a residual catalytic effect of the inner surfaces of the reactor. Despite of these deviations, the agreement between experimental measurements and the model predictions is in general satisfactory, since the effect of both temperature and flow-rate (i.e. residence time τ in the reactor) is well predicted by the model.

This achievement confirms the reliability of the skeletal reduction process and allows for the extension of the experimental database for ethanol oxidation and pyrolysis already available in literature [38]; pyrolysis data and simulations are provided in Supplementary Material S4. The comparison also shows that the predictions of the complete and reduced mechanisms are virtually identical, thus enabling the adoption of the reduced mechanism in coupled homogeneous/heterogeneous simulations of a catalytic reactor with a significant reduction of the computational effort.

These results confirm that in a catalytic ethanol-to-$H_2$ system, not only heterogeneous reactions, but also homogeneous oxidation and thermal cracking can play a role in the formation of products at temperatures higher than 600 °C.

## Development of a heterogenous kinetic scheme

The reactivity of ethanol on $Rh/Al_2O_3$ catalyst was described by following the same lumped approach adopted for developing the kinetics of $CH_4$ [16], formic acid [24] and $C_{2+}$ hydrocarbons [21,22]. This consists of building a kinetic scheme that incorporates all the stoichiometries that are necessary to reproduce the speciation of the reacting system and formulating for each reaction an analytic expression that reflects the dominant kinetic dependences from gas-phase species. In this way a subsystem is created, that can be coupled with existing subsystems that cover the $C_1$–$C_8$ partial oxidation and steam reforming systems [16,21,27]. The reaction rates of this macrokinetic scheme are expressed per unit mass of the catalyst $Rh/Al_2O_3$ ($g_{cat}$).

Catalytic tests were performed to collect the necessary data sets, build the kinetic model and fit the parameters. While data and their analysis are discussed in the following, the final scheme is reported in Table 2. It includes reactions and rate expressions for oxidation and steam reforming of ethanol, along the lines of the previous experience on hydrocarbons CPO over Rh-alumina catalyst; besides, it incorporates oxidative dehydrogenation, dehydrogenation and decomposition reactions that are specific of the $C_2$-alcohol. The complete ethanol scheme includes as relevant subsystem the pre-existing $C_1$ sub-scheme, comprising $CH_4$ total oxidation and SR, WGS (modified by C-poisoning term) and rev-WGS, $H_2$ and CO oxidation, whose rate expressions and parameters were maintained from the original sources [16].

As a consolidated procedure, tests of $CH_4$ CPO were used as benchmark to evaluate the consistency between the pre-existing $C_1$ kinetic scheme and the behaviour of newly prepared catalytic reactors. An example of comparison between

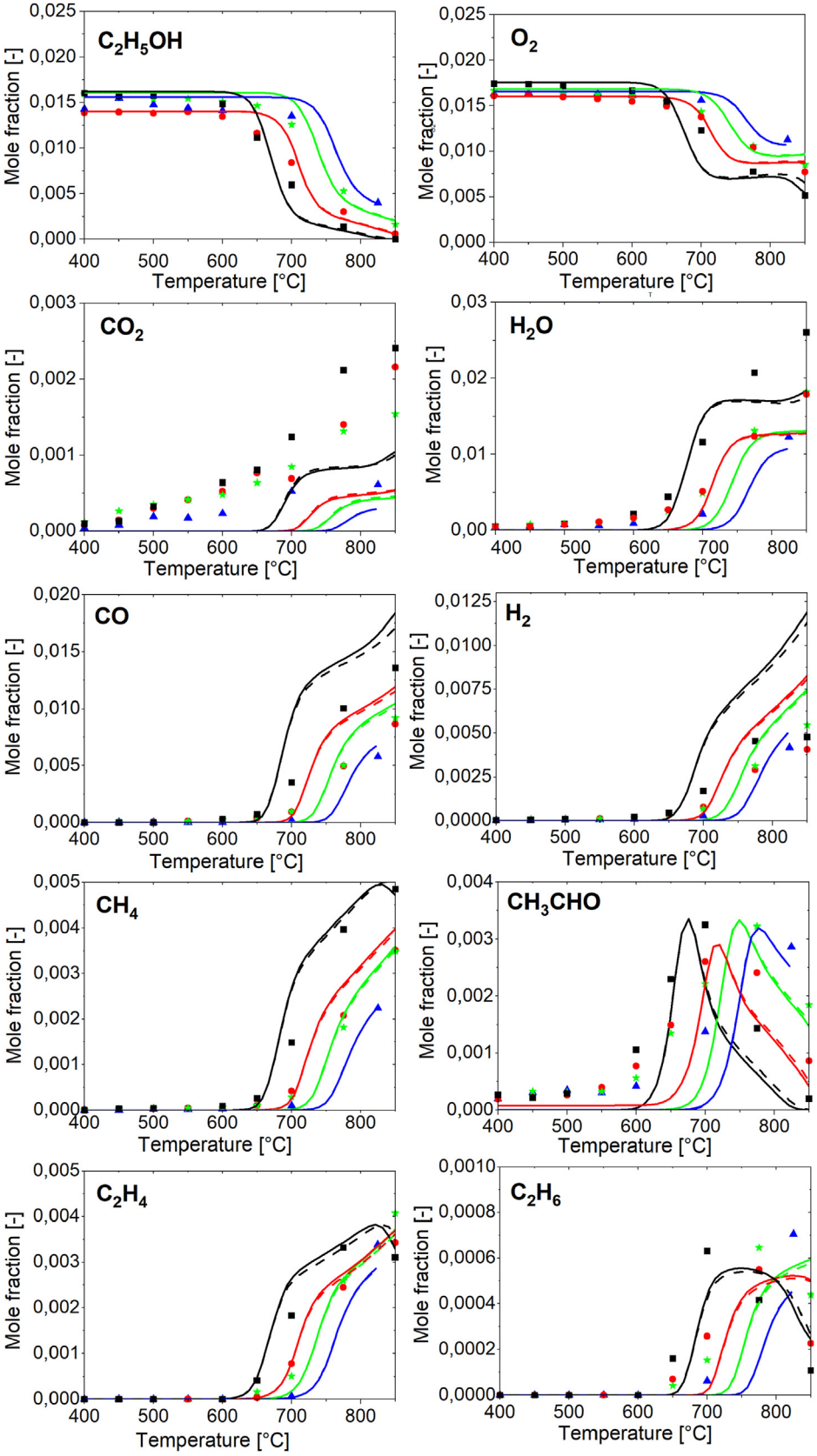


**Fig. 2 – Effect of flowrate on homogeneous ethanol oxidation. Experimental data (symbols), complete model predictions (dashed lines) and 36 species reduced model predictions (solid lines) are reported. Operating conditions: $C_2H_5OH$ = 1.5%, $O_2$ = 1.68%, $N_2$ to balance. Black-squares: flowrate = 225 Nml/min ($\tau$ = 0.19 s); Red-circles: flowrate = 451 Nml/min ($\tau$ = 0.09 s); Green-stars: flowrate = 812 Nml/min ($\tau$ = 0.05 s); Blue-triangles: flowrate = 1334 Nml/min ($\tau$ = 0.03 s). (For interpretation of the references to color in this figure legend, the reader is referred to the Web version of this article.)**

**Table 2 – Reaction scheme of ethanol reactivity on $Rh/Al_2O_3$.**

| Reaction | Rate equation [mol/($g_{cat}$ s)] | $k_{rif,j}^{873K}$ [mol/(atm $g_{cat}$ s)] | $E_{act}$ [kJ/mol] |
|---|---|---|---|
| $C_2H_5OH$ oxidative dehydrogenation<br>$C_2H_5OH + 0.5\ O_2 \rightarrow CH_3CHO + H_2O$ | $r_{ODH} = k_{ODH} \cdot P_{O_2}$ | $3.97 \times 10^{-1}$ | 50 |
| $C_2H_5OH$ dehydrogenation<br>$C_2H_5OH \rightarrow CH_3CHO + H_2$ | $r_{deH} = k_{deH} \cdot P_{C_2H_5OH} \cdot \sigma_{O_2}$ | $3.84 \times 10^{-2}$ | 40 |
| $C_2H_5OH$ total oxidation<br>$C_2H_5OH + 3\ O_2 \rightarrow 2CO_2 + 3H_2O$ | $r_{TO} = \frac{k_{TO} \cdot P_{O_2}}{\left(1 + K_1 \cdot \frac{P_{O_2}}{P_{C_2H_5OH}}\right)^2}$ | $3.209 \times 10^{1}$ [22] | 54 [22] |
| $C_2H_5OH$ decomposition<br>$C_2H_5OH \rightarrow CH_4 + CO + H_2$ | $r_{DEC} = k_{DEC} \cdot P_{C_2H_5OH} \cdot \sigma_{O_2}$ | $7.935 \times 10^{-2}$ | 50 |
| $C_2H_5OH$ steam reforming<br>$C_2H_5OH + H_2O \leftrightarrow 2CO + 4H_2$ | $r_{SR,C_2H_5OH} = \frac{k_{SR_{C_2H_5OH}} \cdot P_{C_2H_5OH} \cdot (1 - \eta_{SR})}{1 + \frac{K_C \cdot P_{C_2H_5OH}}{P_{H_2O}}}$ | $4 \times 10^{-2}$ | 90 |
| $CH_3CHO$ steam reforming<br>$CH_3CHO + H_2O \leftrightarrow 2CO + 3H_2$ | $r_{SR,CH_3CHO} = \frac{k_{SR,CH_3CHO} \cdot P_{CH_3CHO} \cdot (1 - \eta_{SR})}{1 + \frac{K_C \cdot P_{C_2H_5OH}}{P_{H_2O}}}$ | $1.2 \times 10^{-1}$ | 30 |
| WGS<br>$CO + H_2O \leftrightarrow CO_2 + H_2$ | $r_{WGS} = \frac{k_{WGS} \cdot P_{H_2O} \cdot (1 - \eta_{WGS})}{1 + \frac{K_C \cdot P_{C_2H_5OH}}{P_{H_2O}}} \cdot \sigma_{CO}$ | $6.831 \times 10^{-3}$ [21] | 75 [21] |

Where $K_1 = 1.4 \exp\left[\frac{22}{R}\left(\frac{1}{T} - \frac{1}{T_0}\right)\right]$ [22] and $K_C = 11.98 \exp\left[\frac{50}{R}\left(\frac{1}{T} - \frac{1}{T_0}\right)\right]$. Temperature dependence of kinetic constants was expressed with a modified Arrhenius form: $k(T) = k(T_{ref})\exp(-E_{act}/R(1/T - 1/T_{ref}))$. Terms $(1-\eta_j)$ indicate equilibrium constraints, where $\eta_j$ represents the ratio of the experimental reaction quotient $K_{p,j}$ and the thermodynamic equilibrium constant $K_{eq,j}$. Coefficients $\sigma_i$ are needed to account for the extinction of the co-reactant: $\sigma_i = P_i/(P_i + 10^{-6})$.

$CH_4$ CPO experimental results and model predictions is reported in Supplementary Material S5.

### *Steam reforming*

Tests of ethanol SR were carried out at 1.5% ethanol and 3–3.8% $H_2O$ feed contents, at varying GHSV (0.9 and $1.5 \cdot 10^6$ NL/$kg_{cat}$/h). Experimental results are shown in Fig. 3, where ethanol conversion and outlet molar fractions are plotted against the average catalytic bed temperature.

The onset of ethanol conversion is seen at temperatures higher than 500 °C, accompanied by $H_2O$ consumption. The major products are CO and $H_2$, and their molar fractions increase with temperature while approaching equilibrium concentrations. In addition, $CO_2$ is also observed among products; its production can be explained by the onset of the water gas shift reaction. The stoichiometries of steam reforming and WGS can thus explain most of the product composition. At this stage, it is observed that traces of ethylene (maximum 500 ppm), acetaldehyde (maximum 250 ppm) and $CH_4$ (maximum 400 ppm) are also detected among the products; their formation is discussed below.

In a previous study [1], the reactivity of the ethanol/$H_2O$ reacting system on Rh was analyzed by combined activity tests, Raman spectra, *operando* FTIR and TPO measurements. Based on these results, the high-temperature onset of the steam reforming reaction (consistent with an apparent activation energy as high as 180 kJ/mol) has been associated to the hindering effect of adsorbed $C_2$ oxygenated species (including acetaldehyde, acetates, ethoxy species). In turn, such species are believed responsible for C–C coupling reactions eventually leading to the formation of disordered and graphitic C-structures, visible by Raman. Consistently, TPO measurements on spent catalysts allowed to quantify C-deposits and revealed the co-presence of different types of structures, with diverse O-content and interaction with catalytic surface. At higher temperature, though, gasification reactions would consume such species, favouring the full availability of the surface active sites.

This complex picture of C-poisoning can be rendered in kinetic terms by assuming a dynamic equilibrium between formation and consumption of surface C-species, such that the rate of formation depends on the gas-phase concentration of ethanol and the coverage of free sites $\theta$ (Eq. (1)):

$$r_{C-formation} = k_{C,f} \cdot P_{C_2H_5OH} \cdot \theta \quad (1)$$

and the rate of C-consumption depends on the gas-phase concentration of $H_2O$ (the gasification medium) and the surface coverage of C-species $\theta_C$ (Eq. (2)):

$$r_{C-consumption} = k_{C,c} \cdot P_{H_2O} \cdot \theta_C \quad (2)$$

The beneficial effect of $H_2O$ for Rh-based catalysts stability in ethanol-to-$H_2$ processes is widely explained in the literature ([39,40]).

By assuming steady state conditions, and thus equalling the rates of formation $r_{C-formation}$ and consumption $r_{C-consumption}$, the following relationship is obtained between the coverage of free sites and the coverage of C-poisoned sites (Eq. (3)):

$$\frac{\theta_C}{\theta} = \frac{k_{C,f}}{k_{C,c}} \cdot \frac{P_{C_2H_5OH}}{P_{H_2O}} \quad (3)$$

By additionally assuming that C-poisoned sites are the MASI, such that the site balance reduces to (Eq. (4)):

$$\theta + \theta_c = 1 \quad (4)$$

the following expression is obtained (Eq. (5)):

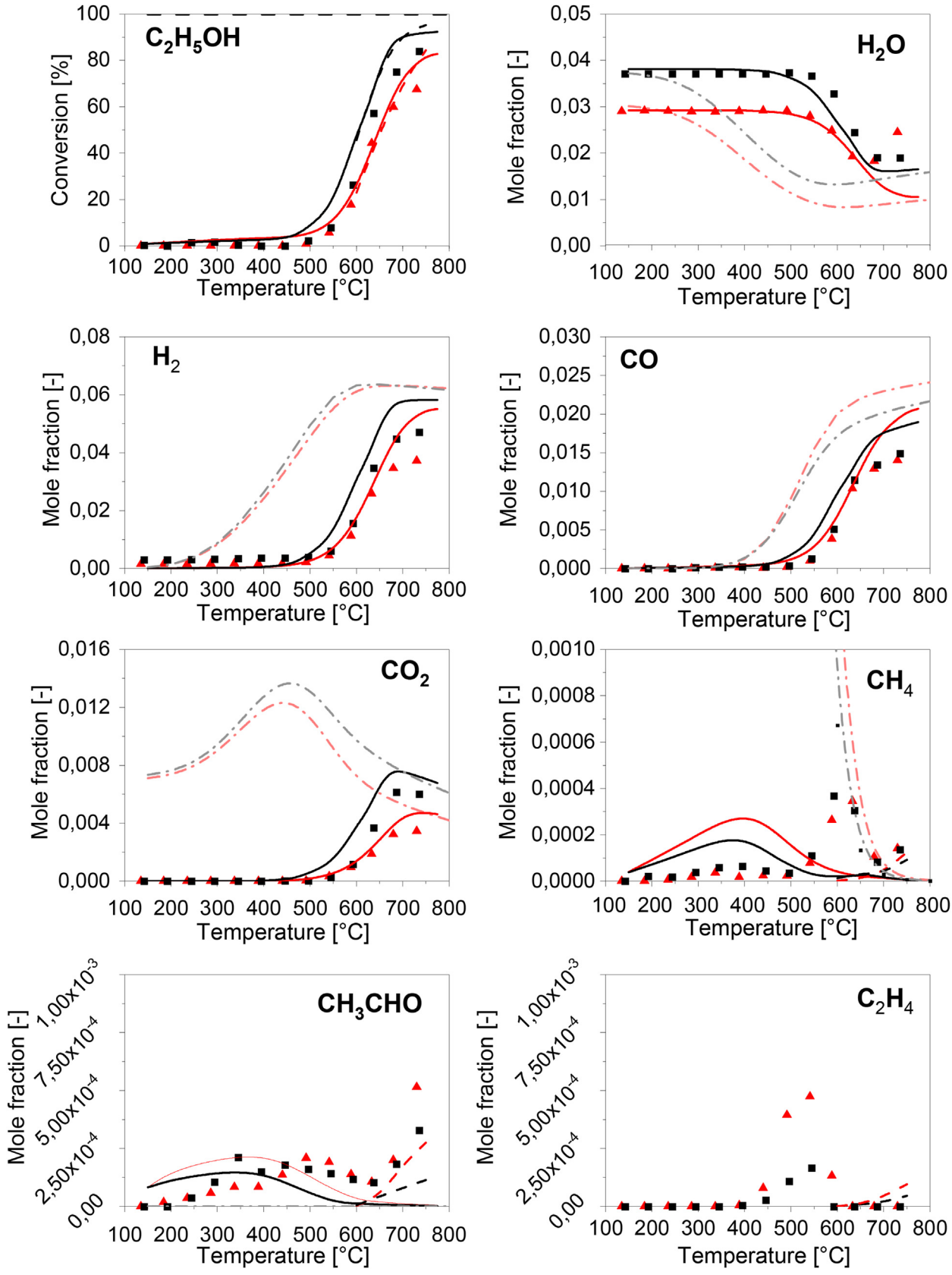


**Fig. 3 – Ethanol SR tests. Experimental data (symbols), heterogeneous model predictions (solid lines), homo/heterogeneous model predictions (dashed lines) and equilibrium compositions (dot-dashed lines) are reported. Operating conditions: $C_2H_5OH$ = 1.5%, $N_2$ to balance. Black-squares: GHSV = $0.9 \cdot 10^6$ NL/$kg_{cat}$/h, $H_2O$ = 3.8%; Red-triangles: GHSV = $1.5 \cdot 10^6$ NL/$kg_{cat}$/h, $H_2O$ = 3%. (For interpretation of the references to color in this figure legend, the reader is referred to the Web version of this article.)**

$$\theta = 1 - \theta_c = \left(1 + \frac{K_C \cdot P_{C_2H_5OH}}{P_{H_2O}}\right)^{-1} \quad (5)$$

where $K_C$ is the lumped parameter, corresponding to the ratio between rate constant of formation $k_{C,f}$ and rate constant of gasification of C-species $k_{C,c}$.

The rate expression of the forward steam reforming was thus obtained by assuming that it is proportional to the partial pressure of ethanol and the surface concentration of free sites, which brings to the following Eq. (6):

$$r_{SR,C_2H_5OH} = k_{SR_{C_2H_5OH}} \cdot P_{C_2H_5OH} \cdot (1 - \theta_c) \cdot (1 - \eta_{SR}) \quad (6)$$

as reported in Table 2.

The term $(1 - \eta_{SR})$ accounts for the approach to equilibrium and conveys thermodynamic consistency.

Notably, the same phenomenology was observed in the study of propylene steam reforming, where the same formalism was successfully adopted [22]. Indeed it has been verified that under the investigated operative conditions CO-poisoning has not a relevant contribution, differently from what was observed by some of the authors for a cleaner fuel as methane [20].

The kinetic parameters of rate expression (Eq. (6)) were adapted to the steam reforming data, accounting also for the WGS reaction. An activation energy of 90 kJ/mol was estimated for the intrinsic rate constant, a value that is comparable with the estimated energy barriers for several fuels so far studied and is considerably lower than the apparent activation energy that emerges when C-poisoning term is not considered [1]. It results higher than the activation energy of propylene, but very similar to that of $CH_4$ and propane SR reactions [16,21,22].

Fig. 3 reports the comparison between model fit (solid lines = incorporation of the heterogeneous scheme) and experimental data, and a very satisfactory description of system composition is observed.

It is also observed that, although not discussed in detail, the model predictions account for a minor formation of $CH_4$ and acetaldehyde in the very intermediate temperature region where these trace species were observed. The simulations were obtained by applying the entire kinetic scheme reported in Table 2, thus including also the O-dependent reactions; indeed, as explained in the experimental methods, the $H_2O$ feed to the annular reactor was obtained by a dedicated upstream unit, consisting of Pt-containing packed bed reactor fed by slightly over stoichiometric $H_2/O_2$ mixtures. A minor slip of $O_2$ (about 50 ppm) was detected by GC analysis from the Pt reactor; by accounting for such small amount of $O_2$ in the SR feed, a little contribution from oxidative reactions was predicted leading to the formation of $CH_4$ (via ethanol oxidative decomposition) and acetaldehyde (via oxidative dehydrogenation).

Fig. 3 also reports the simulations obtained by combining the homogeneous and the heterogeneous scheme (dotted lines = incorporation of both kinetic schemes). Apparently, gas-phase reactions had a negligible impact; however, interestingly, homogenous reactions can explain the very high temperature formation of traces of acetaldehyde and methane. Also traces of ethylene were predicted at high temperature, although not detected in the reactor outlet.

As a further support to the SR kinetics, it is mentioned that additional data of ethanol steam reforming were simulated, including tests at lower $H_2O$ content where C-poisoning was emphasized and tests that were performed in rapidly descending ramps from high temperatures, in the attempt to contrast the formation of C-species. The additional experimental results are reported in the Supplementary Material S6 together with the model predictions; a good agreement was found, which is highly satisfactory when considering the simplicity of the kinetic expression introduced.

Finally, it is worth emphasizing that, consistently with the SR kinetics, a correction by surface C-poisoning was applied to the water gas shift reaction (as shown in Table 2). Indeed, the productivity of $CO_2$ herein observed was largely lower than expected based on the original studies by Donazzi et al. [16] and Pagani et al. [21]. Instead, as shown by the solid lines in Fig. 3, a very satisfactory description was obtained by assuming that the same hindering effect of C-forming reactions similarly reduces the available sites for the WGS reaction, whose rate equation and intrinsic parameters were maintained unchanged.

### *Catalytic partial oxidation*

An extensive discussion on the multiple reaction pathways observed in ethanol CPO has been addressed in Ref. [1], and is here briefly summarized. Reference CPO data (with ethanol and $O_2$ feed content of 1.5% and 1.68%, respectively, and GHSV of 5 and $9 \cdot 10^5$ NL/$kg_{cat}$/h) are reported in Fig. 4, in terms of ethanol and oxygen conversion and molar fractions of the reaction products. In the low temperature range (T < 200 °C) ethanol oxidative dehydrogenation to acetaldehyde is responsible for the initial conversion of reactants; the remarkable feature revealed by the tests in annular reactor at high space velocity is that this reaction extinguishes at increasing temperature, since acetaldehyde concentration and ethanol conversion pass through maxima.

Ethanol total oxidation to $CO_2$ and $H_2O$ and ethanol oxidative decomposition to $CH_4$, CO and $H_2$ are instead activated above 250 °C. As long as $O_2$ is present on the surface, these species are subjected to post-oxidation reactions; $CH_4$ formation likely contributes to the medium temperature production of $H_2$ and CO, via consecutive steam reforming (that according to our previous studies is active only if $O_2$ is consumed [16]).

Still in the intermediate temperature range a secondary formation of acetaldehyde is observed, likely associated to a dehydrogenation route possibly occurring on the support. Other experiments prove that the importance of this reactivity is strictly related to the $\gamma$-$Al_2O_3$ batch utilized for catalyst preparation; in this respect, Le Valant and co-workers in Ref. [41] state that this reactivity is correlated to the basicity of the support.

In line with ethanol SR experiments, the onset of ethanol reforming (with important production of CO and $H_2$, together with ethanol and water consumption increase) is delayed at temperatures higher than 500 °C. The two runs reported in

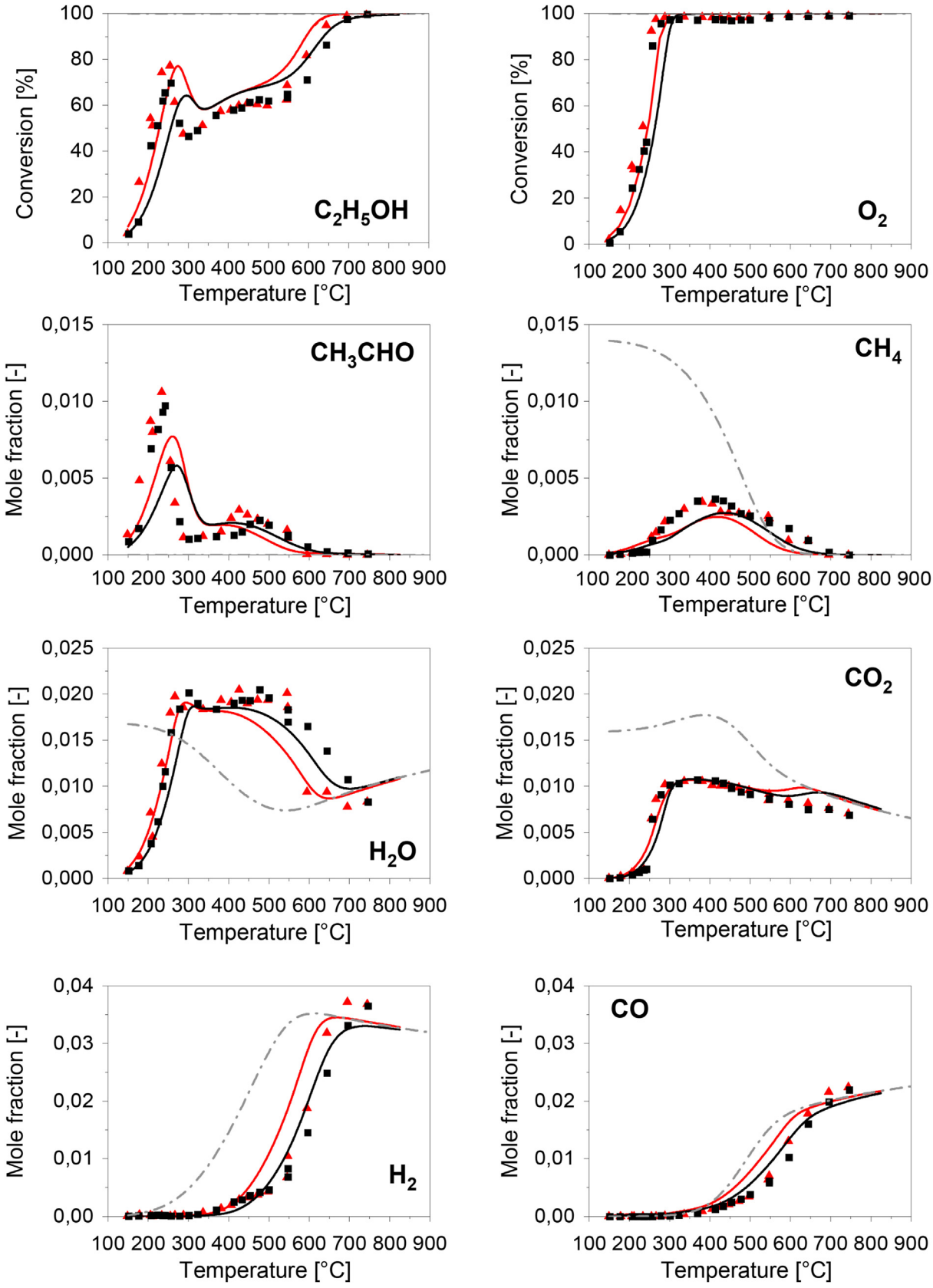


**Fig. 4 – Ethanol CPO tests. Experimental data (symbols), heterogeneous model predictions (solid lines) and equilibrium compositions (dot-dashed lines) are reported. Operating conditions: $C_2H_5OH$ = 1.5%, $O_2$ = 1.68%, $N_2$ to balance. Black-squares: GHSV = $9{\cdot}10^5$ NL/$kg_{cat}$/h; Red-triangles: GHSV = $5{\cdot}10^5$ NL/$kg_{cat}$/h. (For interpretation of the references to color in this figure legend, the reader is referred to the Web version of this article.)**

Fig. 4 show that in the intermediate T-range, in between 300 and 500 °C, ethanol conversion presents a sort of "plateau-like" behaviour which is in line with the hypothesis that once $O_2$ is fully consumed, a C-poisoned regime similar to SR system causes the delayed ignition of ethanol reforming. At the maximum temperature of 775 °C – for the highest GHSV of $9{\cdot}10^5$ NL/$kg_{cat}$/h – the observed C selectivity to CO and H selectivity to $H_2$ are around 78%, with a total ethanol conversion of 100%.

All these stoichiometries were incorporated in the kinetic scheme of Table 2 and kinetic dependences were formulated based on an extensive experimental campaign of ethanol CPO tests at varying feed composition and space velocity (Supplementary Material S7). Similarly to steam reforming, the proposed rate expressions respect the analogy with the kinetics of other fuels studied in the past as well as the search for simple analytic expressions.

The kinetics of the low temperature oxidative dehydrogenation to acetaldehyde and water was described by assuming a direct dependence on the gas-phase concentration of $O_2$. Indeed, on the one side this unique route is observed only in $O_2$ co-feed tests, on the other side the "extinction" above 200 °C can be explained by the rapid depletion of $O_2$, due to the onset of deep oxidation. The following kinetic expression has been introduced to describe acetaldehyde "peak" (Eq. (7)):

$$r_{ODH} = k_{ODH} \cdot P_{O_2} \tag{7}$$

where it is assumed that ethanol oxidative dehydrogenation is not impacted by ethanol concentration, which presumably reaches a saturation value on the surface, but rather by $O_2$ partial pressure.

The key role of surface $O_2$ availability on oxidative dehydrogenation reaction together with the limited influence of GHSV on acetaldehyde production suggest that the reaction is associated with a specific nature of adsorbed oxygen, possibly undissociated Rh–$O_2$, from which RhO* sites (typically involved in the deep oxidation activity) originate. Such Rh–$O_2$ sites might be present on the catalytic surface in limited amount (e.g. on Rh/support interface) and characterized by a vivid H-abstraction activity. It is also suggested that ethanol oxidative dehydrogenation requires the vicinal interaction of both $O_2$ and ethanol molecules on the surface, i.e. the presence of vicinal Rh–$O_2$ and $C_2H_5OH$*.

By virtue of the similar consumption trend of ethanol compared to propylene, the same reaction rate expression was chosen to describe ethanol total oxidation over Rh catalysts, here reported in Eq. (8) [22]:

$$r_{TO} = \frac{k_{TO} \cdot P_{O2}}{\left(1 + K_1 \cdot \frac{P_{O2}}{P_{C_2H_5OH}}\right)^2} \tag{8}$$

A negative dependence on $O_2$ and a second order dependence on the fuel partial pressure were thus assumed. In analogy with the case of propylene, the macro-kinetic dependencies in Eq. (8) can be estimated by assuming a kinetic regime similar to the one proposed by Iglesia and co-authors in Refs. [42–44]: the rate determining step in the activation of the fuel is assumed as the dissociative adsorption on the pair Rh–RhO* sites, being the adsorbed molecular oxygen irreversibly dissociated into atomic O*; due to the very high reactivity of the fuel, the surface concentration of O* species would result from the dynamic equilibrium between $O_2$ adsorption and surface oxygen consumption by deep oxidation. Indeed, the pre-exponential factor and the activation energy of $k_{TO}$, the parameter representative of $O_2$ activation, were kept equal to the values proposed in Ref. [22], with a pre-exponential factor of 32.1 mol/(atm· $g_{cat}$ ·s) at 873 K and an activation energy of 54 kJ/mol. The global parameter $K_1$ at the denominator is instead the ratio between $k_{TO}$ and the rate constant of O* consumption. Also the parameters for the evaluation of this term were mantained the same as those of propylene [22], showing to be more dependent on the process of $O_2$ activation rather than the fuel nature.

In order to account for the formation of methane observed in the intermediate temperature range, a catalytic decomposition of ethanol was introduced. As shown in the proposed reaction rate for decomposition (Eq (9)), a simple first order dependence on fuel partial pressure was chosen.

$$r_{DEC} = k_{DEC} \cdot P_{C_2H_5OH} \cdot \sigma_{O2} \tag{9}$$

A value of activation energy of 50 kJ/mol was estimated, as reported in Table 2. This reaction route was also observed by A. Cifuentes et al. [45] in the low temperature range over Rh–Pd/$CeO_2$ catalyst, where a higher activation energy was evaluated (87 kJ/mol). Plots of methane concentration in Fig. 4 show a trend through a maximum peak: C–C bond breaking to methane rate becomes null when oxygen is fully consumed in the system, thus a term $\sigma_{O_2}$ was introduced to guarantee a numerical dependence on $O_2$ partial pressure. In fact, ethanol decomposition to methane was identified as a more intensive phenomenon with $O_2$ in the reacting mixture, while the production of methane was observed in trace amounts in the steam reforming tests. Indeed, as shown in Ref. [1], *operando* IR analyses in ethanol CPO clearly showed the C–C bond cleavage is significantly more favoured in the presence of $O_2$ co-feed rather than $H_2O$ co-feed. The presence of a maximum of methane concentration at increasing temperature can be partly explained also by the onset of consecutive reactions (namely oxidation and steam reforming); this is the reason why the ethanol scheme needs a close integration with the $C_1$-scheme, which also involves all the reactions related to the syngas chemistry (water gas shift, reverse water gas shift, methanation), all of them described by reversible rate equations to respect the thermodynamic consistency.

Also a minor formation of acetaldehyde was observed in the middle temperatures range, whose formation was accounted for through a dehydrogenation reaction of ethanol. Data analysis showed a dependence on ethanol inlet partial pressure (Supplementary Material S7), thus leading to the reaction rate expression reported in the following Eq. (10), where a simple first order dependence on ethanol partial pressure is proposed:

$$r_{deH} = k_{deH} \cdot P_{C_2H_5OH} \cdot \sigma_{O_2} \tag{10}$$

Differently from the low-temperature formation of acetaldehyde, the bulk of experiments seems to suggest that this secondary contribution of formation is more influenced by the residual concentration of ethanol. As already discussed for decomposition reaction, $\sigma_{O_2}$ term was introduced to make the

reactivity null when oxygen is completely depleted. Indeed, ethanol SR experiments showed that ethanol dehydrogenation is not significantly active in the absence of $O_2$.

High-temperature behaviour of ethanol in CPO is explained by the onset of ethanol steam reforming, which justifies the observed consumption of $H_2O$ and residual ethanol. The ethanol reforming reactivity previously presented was hence introduced in the complete kinetic scheme for ethanol CPO, maintaining the same rate expression with C-poisoning. Indeed, as in the case of ethanol SR system, also in CPO the onset of reforming takes place at temperatures much higher than $O_2$ consumption. An equivalent state of surface coverages is then expected for both ethanol CPO and SR [24].

In analogy with ethanol steam reforming kinetic, a reaction of acetaldehyde steam reforming was introduced (Eq. (11)):

$$r_{SR,CH_3CHO} = \frac{k_{SR_{CH_3CHO}} \cdot P_{CH_3CHO} \cdot (1 - \eta_{SR})}{1 + \frac{K_c \cdot P_{C_2H_5OH}}{P_{H2O}}} \quad (11)$$

All the newly introduced kinetic parameters were estimated by fitting the whole population of SR and CPO data. Figs. 3 and 4 show the satisfactory description obtained by the model in

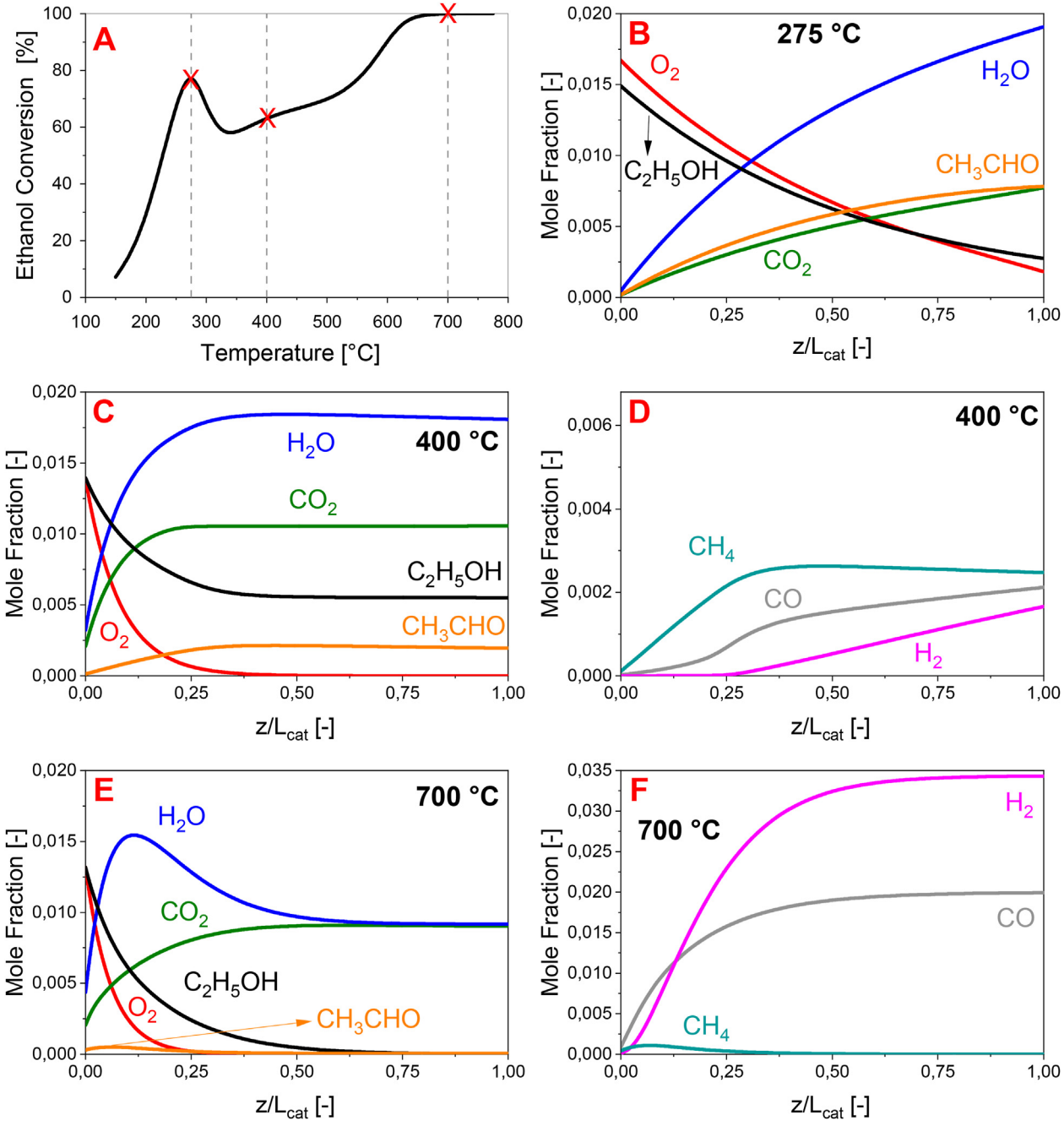


**Fig. 5 – Modelling results of ethanol CPO. Inlet composition: $C_2H_5OH$ = 1.5%, $O_2$ = 1.68%, $N_2$ to balance. GHSV = $5{\cdot}10^5$ NL/$kg_{cat}$/h. Panel A: Ethanol Conversion. Panels B–C–D–E–F: axial evolution of gas-phase species molar fractions along the adimensional reactor coordinate at varying temperature (indicated).**

solid lines. Further experimental data and model simulations are reported in Supplementary Material S6 and S7.

Similarly to the case of SR, also the CPO data were simulated with and without inclusion of the homogeneous scheme; no appreciable contribution from the thermal conversion of ethanol was appreciated, and for this reason homo/heterogeneous model predictions were not reported in the plots. Indeed, even if in the validation of the reduced homogeneous scheme it was shown a role of gas phase reactions above 600 °C, in the presence of the catalytic phase they are significantly hindered because of the fast oxygen depletion.

## Micro-reactor analysis

Integral performances were so far discussed and fitted with the model; in order to fully appreciate the interconnection of ethanol conversion routes and the implications on the final reactor performance, the reactor and kinetic model can be also used to visualize the axial evolution of species molar fractions, as presented in Fig. 5, where model simulations of ethanol CPO are shown. These profiles are shown for three temperatures that capture different reaction regimes and ethanol conversion values (Fig. 5A). At 275 °C ethanol conversion reaches a local maximum: ethanol reacts along the axis together with $O_2$ and the products that evolve are acetaldehyde, $H_2O$ and $CO_2$, corresponding to the stoichiometry of oxidative dehydrogenation, whose integral rate is expected to be maximal here, and of total oxidation (Fig. 5B). The kinetic dependences are such that acetaldehyde tends to flatten across the bed, while oxygen is being consumed. Water is here the most abundant reaction product. In Fig. 5C, at 400 °C, the full onset of deep oxidation is depicted and total oxidation prevails over other reactions. The conversion of $O_2$ (the limiting reactant) and ethanol is concentrated at the bed entrance and the products reach a plateau, while other oxidative reactions lead to acetaldehyde, $CH_4$, CO, and $H_2$ which evolve in small amounts from the catalytic surface in the gas-phase (Fig. 5D). High temperatures are needed to boost the gasification of adsorbed C-species and the consecutive promotion of steam reforming. Indeed, at 700 °C (Fig. 5E/F) ethanol reaches complete conversion, water concentration passes through a maximum and $H_2$ concentration grows along the axial coordinate, being the most important reaction product at the reactor outlet.

The reactor operation at high temperature emerges thus as the unique solution for the production of $H_2$-rich streams in real fuel processors. Still, intermediate regimes can be passed through during dynamic operations of the reactor (e.g. light-off, shut-down) that might be of importance especially in the case of distributed, small-scale $H_2$ production units. The availability of engineering models able to describe the evolution of the reaction system and the product speciation at varying conditions is of the utmost importance for properly designing the reactor and the operation strategies.

## Conclusions

This work focuses on the development of an engineering tool that captures all the relevant features of ethanol partial oxidation and steam reforming reacting systems: a combined homogeneous-heterogeneous kinetic scheme has been developed and validated against experimental data, informative of the catalytic and thermal activation of the $C_2$-alcohol.

Gas-phase reactions can affect the product distribution at temperatures higher than 600 °C, but are strongly dependent on the concentration of $O_2$. In the presence of the catalytic phase, where $O_2$ is typically consumed by fast oxidation reactions, the possible coexistence of gas-phase reaction is limited to very high temperatures. The study presents a reduced homogeneous scheme, based on 36 reacting species, thus a very flexible tool that can reproduce the observed trends with a limited computational load.

The catalytic activation of ethanol covers instead a very broad temperature window. The dominant catalytic routes pass from selective oxidation to acetaldehyde below 200 °C to deep oxidation and oxygen-assisted decomposition above 250 °C, while the onset of ethanol steam reforming is observed above 500 °C. Based on the kinetic tests herein collected and the previous spectroscopic investigations, the hindering effect of ethanol adsorption on the catalyst and surface C-formation has been introduced in the model. This C-poisoning factor mitigates with increasing temperature and concentration of $H_2O$, and this justifies the remarkable apparent activation energy of ethanol steam reforming.

The heterogeneous macro-kinetic scheme herein proposed consists of six molecular reactions that, combined with the previously developed $C_1$-subsystem ($CH_4$ oxidation and steam reforming, water gas shift and reverse water gas shift, CO and $H_2$ consecutive oxidations) and the homogeneous reduced scheme, can describe with a high level of accuracy the ethanol/$O_2$ and ethanol/$H_2O$ reacting systems.

## Declaration of competing interest

The authors declare that they have no known competing financial interests or personal relationships that could have appeared to influence the work reported in this paper.

## Acknowledgement

This research has received funding from Politecnico di Milano (PoliMI PhD scholarship to V. Troisi), from ENI S. p.A. (PhD scholarship to V. Piazza) and from Dipartimento di Energia, Politecnico di Milano, within *Energy for Motion* program.

## Appendix A. Supplementary data

Supplementary data to this article can be found online at https://doi.org/10.1016/j.ijhydene.2023.03.178.

## Notation

| | |
|---|---|
| $C_{TOT}$ | total concentration (mol $m^{-3}$) |
| $d_h$ | hydraulic diameter (m) |

$D_i$ molecular diffusivity of species $i$ ($m^2\ s^{-1}$)
$F_i$ molar flow of species $i$ (mol $s^{-1}$)
$F_i^*$ dimensionless molar flow of species $i$ $F_i^* = \frac{F_i}{F_{TOT}^0}$
$F_{TOT}^0$ total inlet molar flow (mol $s^{-1}$)
$F_{TOT}$ total molar flow (mol $s^{-1}$)
$K_{c,i}$ mass transfer coefficient of species $i$ (m $s^{-1}$)
$m_{cat}$ catalyst weight (g)
$Pe_{m,i}$ Péclet number $Pe_{m,i} = ReSc_i$
$P_i$ partial pressure of species $i$ (atm)
$r_j$ Rate of reaction j (mol $s^{-1}$ $g_{cat}^{-1}$)
$Re$ Reynolds number $Re = \frac{v d_h}{\nu}$
$R_{ext}$ external radius of annular section (m)
$R_{int}$ internal radius of annular section (m)
$S$ geometrical surface area of the catalyst ($m^2$)
$Sc_i$ Schmidt number of species $i$ $Sc_i = \frac{\nu}{D_i}$
$Sh_{loc,i}$ local Sherwood number of species $i$ $Sh_{loc,i} = \frac{K_{c,i} d_h}{D_i}$
$x_i^B$ bulk molar fraction of species $i$
$x_i^W$ wall molar fraction of species $i$
$z$ axial coordinate
$z^*$ dimensionless axial coordinate $z^* = \frac{z}{d_h}$

*Greek symbols*

$\delta_L$ thickness of the catalytic layer (m)
$\nu_i$ cinematic viscosity of species $i$ ($m^2\ s^{-1}$)
$\nu_{i,j}$ stoichiometric coefficient of species $i$ in the $j$ reaction
$\sigma_i$ Limiting factor for species $i$ $\sigma_i = P_i/(P_i + 10^{-6})$
$\Phi_i$ generalized Thiele modulus of species $i$

## REFERENCES


[1] Piazza V, Junior RBS, Luccisano G, Pietrogiacomi D, Groppi G, Gazzoli D, Beretta A. $H_2$ from biofuels and carriers: gas-phase and surface ethanol conversion pathways on $Rh/Al_2O_3$ investigated by annular microreactor coupled with Raman and FTIR spectroscopy. J Catal 2022;413:184–200. https://doi.org/10.1016/j.jcat.2022.06.012.

[2] Bartholomew CH. Mechanisms of catalyst deactivation. 2001.

[3] Vaidya PD, Rodrigues AE. Kinetics of steam reforming of ethanol over a $Ru/Al_2O_3$ catalyst. Ind Eng Chem Res 2006;45(19):6614–8. https://doi.org/10.1021/ie051342m.

[4] Gorke O, Pfeifer P, Schubert K. Kinetic study of ethanol reforming in a microreactor. Appl Catal Gen 2009;360(2):232–41. https://doi.org/10.1016/j.apcata.2009.03.026.

[5] Graschinsky C, Laborde M, Amadeo N, Le Valant A, Bion N, Epron F, Duprez D. Ethanol steam reforming over Rh(1%) $MgAl_2O_4/Al_2O_3$: a kinetic study. Ind Eng Chem Res 2010;49(24):12383–9. https://doi.org/10.1021/ie101284k.

[6] Graschinsky C, Contreras JL, Amadeo N, Laborde M. Ethanol oxidative steam reforming over $Rh(1\%)/MgAl_2O_4/Al_2O_3$ catalyst. Ind Eng Chem Res 2014;53:15348–56. https://doi.org/10.31857/s0044457x21080298.

[7] Peela NR, Kunzru D. Oxidative steam reforming of ethanol over Rh based catalysts in a micro-channel reactor. Int J Hydrogen Energy Mar. 2011;36(5):3384–96. https://doi.org/10.1016/j.ijhydene.2010.12.091.

[8] Sawatmongkhon B, Theinnoi K, Wongchang T, Haoharn C, Wongkhorsub C, Sukjit E. Modeling of hydrogen production from catalytic partial oxidation of ethanol over a platinum-rhodium-supported catalyst. Energy Fuel 2021;35(5):4404–17. https://doi.org/10.1021/acs.energyfuels.0c04125.

[9] Lu T, Law CK. Toward accommodating realistic fuel chemistry in large-scale computations. Prog Energy Combust Sci 2009;35(2):192–215. https://doi.org/10.1016/j.pecs.2008.10.002.

[10] Cuoci A, Frassoldati A, Faravelli T, Ranzi E. OpenSMOKE++: an object-oriented framework for the numerical modeling of reactive systems with detailed kinetic mechanisms. Comput Phys Commun 2015;192:237–64. https://doi.org/10.1016/j.cpc.2015.02.014.

[11] Stewart GW. The decompositional approach to matrix computation. Comput Sci Eng 2000;2(1):50–9.

[12] Mostafa A, Uysal Y, Junior RBS, Beretta A, Groppi G. Catalytic partial oxidation of ethanol over Rh-coated monoliths investigated by the axially resolved sampling technique: effect of $H_2O$ co-feed. Catal Today 2021;367(April 2020):71–82. https://doi.org/10.1016/j.cattod.2020.09.030.

[13] Beretta A, Donazzi A, Groppi G, Forzatti P, Del Santo V, Sordelli L, De Grandi V, Psaro R. Testing in annular micro-reactor and characterization of supported Rh nanoparticles for the catalytic partial oxidation of methane: effect of the preparation procedure. Appl Catal, B 2008;83(1–2):96–109. https://doi.org/10.1016/j.apcatb.2008.02.007.

[14] Beretta A, Bruno T, Groppi G, Tavazzi I, Forzatti P. Conditioning of $Rh/\alpha\text{-}Al_2O_3$ catalysts for $H_2$ production via $CH_4$ partial oxidation at high space velocity. Appl Catal, B 2007;70(1–4):515–24. https://doi.org/10.1016/j.apcatb.2006.01.014.

[15] Bruno T, Beretta A, Groppi G, Roderi M, Forzatti P. A study of methane partial oxidation in annular reactor: activity of $Rh/\alpha\text{-}Al_2O_3$ and $Rh/ZrO_2$ catalysts. Catal Today 2005;99(1–2):89–98. https://doi.org/10.1016/j.cattod.2004.09.027.

[16] Donazzi A, Beretta A, Groppi G, Forzatti P. Catalytic partial oxidation of methane over a 4% $Rh/\alpha\text{-}Al_2O_3$ catalyst. Part I: kinetic study in annular reactor. J Catal 2008;255(2):241–58. https://doi.org/10.1016/j.jcat.2008.02.009.

[17] Beretta A, Tronconi E, Forzatti P, Pasquon I, Micheli E, Tagliabue L, Antonelli GB. Development of a mechanistic kinetic model of the higher alcohol synthesis over a Cs-doped Zn/Cr/O catalyst. Model derivation and data fitting. Ind Eng Chem Res 1996;35(7):2144–53. https://doi.org/10.1021/ie9506173.

[18] Beretta A, Baiardi P, Prina D, Forzatti P. Development of a catalytic reactor with annular configuration118. Elsevier Masson SAS; 1998. https://doi.org/10.1016/s0167-2991(98)80220-6.

[19] Beretta A, Baiardi P, Prina D, Forzatti P. Analysis of a catalytic annular reactor for very short contact times. Chem Eng Sci 1999;54(6):765–73. https://doi.org/10.1016/S0009-2509(98)00261-9.

[20] Donazzi A, Beretta A, Groppi G, Forzatti P. Catalytic partial oxidation of methane over a 4% $Rh/\alpha\text{-}Al_2O_3$ catalyst Part II: role of CO2 reforming. J Catal 2008;255(2):259–68. https://doi.org/10.1016/j.jcat.2008.02.010.

[21] Pagani D, Livio D, Donazzi A, Beretta A, Groppi G, Maestri M, Tronconi E. A kinetic. analysis of the partial oxidation of $C_3H_8$ over a 2% $Rh/Al_2O_3$ catalyst in annular microreactor. Catal Today 2012;197(1):265–80. https://doi.org/10.1016/j.cattod.2012.09.004.

[22] Pagani D, Livio D, Donazzi A, Maestri M, Beretta A, Groppi G, Forzatti P. A kinetic investigation of the catalytic partial oxidation of propylene over a $Rh/Al_2O_3$ catalyst. Ind Eng Chem Res 2014;53(5):1804–15. https://doi.org/10.1021/ie4025352.

[23] Pagani D, Silva Junior RB, Moioli E, Donazzi A, Lucotti A, Tommasini M, Castiglioni C, Brandao ST, Beretta A, Groppi G. Annular reactor testing and Raman surface characterization of the CPO of i-octane and n-octane on Rh based catalyst.

Chem Eng J 2016;294:9–21. https://doi.org/10.1016/j.cej.2016.02.090.
[24] Piazza V, Silva Junior RB, Gazzoli D, Groppi G, Beretta A. $H_2$ from biofuels and carriers: a kinetic investigation of formic acid decomposition on $Rh/Al_2O_3$ in the annular reactor. Chem Eng Res Des 2022;181:458–72. https://doi.org/10.1016/j.cherd.2022.03.048.
[25] Silva Junior RB, Brandao ST, Lucotti A, Tommasini MS, Castiglioni C, Groppi G, Beretta A. Chemical pathways in the partial oxidation and steam reforming of acetic acid over a $Rh-Al_2O_3$ catalyst. Catal Today 2017;289:162–72. https://doi.org/10.1016/j.cattod.2016.08.018.
[26] "StanJan", bioanalytical microfluids program (accessed 2022), https://navier.engr.colostate.edu/code/code-4/index.html.
[27] Donazzi A, Beretta A, Groppi G, Forzatti P. Catalytic partial oxidation of methane over a 4% $Rh/\alpha-Al_2O_3$ catalyst Part II: role of $CO_2$ reforming. J Catal 2008;255(2):259–68. https://doi.org/10.1016/j.jcat.2008.02.010.
[28] Ranzi E, Cavallotti C, Cuoci A, Frassoldati A, Pelucchi M, Faravelli T. New reaction classes in the kinetic modeling of low temperature oxidation of n-alkanes. Combust Flame 2015;162(5):1679–91. https://doi.org/10.1016/j.combustflame.2014.11.030.
[29] Metcalfe WK, Burke SM, Ahmed SS, Curran HJ. A hierarchical and comparative kinetic modeling study of $C_1$ - $C_2$ hydrocarbon and oxygenated fuels. Int J Chem Kinet 2013;45(10):638–75. https://doi.org/10.1002/kin.20802.
[30] Burke SM, Burke U, Mc Donagh R, Mathieu O, Osorio I, Keesee C, Morones A, Petersen EL, Wang W, DeVerter TA, Oehlschlaeger MA, Rhodes B, Hanson RK, Davidson DF, Weber BW, Sung CJ, Santner J, Ju Y, Haas FM, Dryer FL, Volkov EN, Nilsson EJK, Konnov AA, Alrefae M, Khaled F, Farooq A, Dirrenberger P, Glaude PA, Battin-Leclerc F, Curran HJ. An experimental and modeling study of propene oxidation. Part 2: ignition delay time and flame speed measurements. Combust Flame 2015;162(2):296–314. https://doi.org/10.1016/j.combustflame.2014.07.032.
[31] Burcat A, Branko R. Third millennium ideal gas and condensed phase thermochemical database for combustion with updates from active thermochemical tables. 2005. https://doi.org/10.2172/925269. Technical Report, vol. ANL-05/20, no. September, p. ANL-05/20 TAE 960.
[32] CreckModeling. http://creckmodeling.chem.polimi.it.
[33] Stagni A. Implementation of detailed chemistry in large-scale combustion computations - PhD Thesis. 2016. https://doi.org/10.1109/IEMBS.2004.1404351.
[34] Pepiot-Desjardins P, Pitsch H. An efficient error-propagation-based reduction method for large chemical kinetic mechanisms. Combust Flame 2008;154(1–2):67–81. https://doi.org/10.1016/j.combustflame.2007.10.020.
[35] Niemeyer KE, Sung CJ, Raju MP. Skeletal mechanism generation for surrogate fuels using directed relation graph with error propagation and sensitivity analysis. Combust Flame 2010;157(9):1760–70. https://doi.org/10.1016/j.combustflame.2009.12.022.
[36] Alzueta MU, Hernandez JM. Ethanol oxidation and its interaction with nitric oxide. Energy Fuel 2002;16(1):166–71. https://doi.org/10.1021/ef010153n.
[37] Stagni A, Schmitt S, Pelucchi M, Frassoldati A, Kohse-Hoinghaus K, Faravelli T. Dimethyl ether oxidation analyzed in a given flow reactor: experimental and modeling uncertainties. Combust Flame Jun. 2022;240. https://doi.org/10.1016/j.combustflame.2022.111998.
[38] Frassoldati A, Cuoci A, Faravelli T, Ranzi E. Kinetic modeling of the oxidation of ethanol and gasoline surrogate mixtures. Combust Sci Technol 2010;182(7):653–67. https://doi.org/10.1080/00102200903466368.
[39] da Silva AM, Mattos Lv, Munera J, Lombardo E, Noronha FB, Cornaglia L. Study of the performance of $Rh/La_2O_3-SiO_2$ and $Rh/CeO_2$ catalysts for SR of ethanol in a conventional fixed-bed reactor and a membrane reactor. Int J Hydrogen Energy 2015;40(11):4154–66. https://doi.org/10.1016/j.ijhydene.2015.01.106.
[40] Moraes TS, Borges LEP, Farrauto R, Noronha FB. Steam reforming of ethanol on $Rh/SiCeO_2$ washcoated monolith catalyst: stable catalyst performance. Int J Hydrogen Energy Jan. 2018;43(1):115–26. https://doi.org/10.1016/j.ijhydene.2017.10.180.
[41] Le Valant A, Can F, Bion N, Duprez D, Epron F. Hydrogen production from raw bioethanol steam reforming : optimization of catalyst composition with improved stability against various impurities. Int J Hydrogen Energy 2010;35(10):5015–20. https://doi.org/10.1016/j.ijhydene.2009.09.008.
[42] Chin YH, Buda C, Neurock M, Iglesia E. Selectivity of chemisorbed oxygen in C-H bond activation and CO oxidation and kinetic consequences for $CH_4-O_2$ catalysis on Pt and Rh clusters. J Catal 2011;283(1):10–24. https://doi.org/10.1016/j.jcat.2011.06.011.
[43] Chin YH, Buda C, Neurock M, Iglesia E. Reactivity of chemisorbed oxygen atoms and their catalytic consequences during $CH_4-O_2$ catalysis on supported Pt clusters. J Am Chem Soc 2011;133(40):15958–78. https://doi.org/10.1021/ja202411v.
[44] Wei J, Iglesia E. Structural requirements and reaction pathways in methane activation and chemical conversion catalyzed by rhodium. J Catal 2004;225(1):116–27. https://doi.org/10.1016/j.jcat.2003.09.030.
[45] Cifuentes A, Torres R, Llorca J. Modelling of the ethanol steam reforming over $Rh-Pd/CeO_2$ catalytic wall reactors. Int J Hydrogen Energy 2020;45(49):26265–73. https://doi.org/10.1016/j.ijhydene.2019.11.034.